RSC Advances

PAPER

View Article Online
View Journal | View Issue

Cite this: *RSC Adv.*, 2018, **8**, 25819

The crystallization kinetics of Co doping on Ni–Mn–Sn magnetic shape memory alloy thin films

Changlong Tan,*[a] Jiachen Zhu,[a] Zhenhua Wang,[a] Kun Zhang,[a] XiaoHua Tian[a] and Wei Cai[b]

Received 30th May 2018
Accepted 10th July 2018

DOI: 10.1039/c8ra04618b

rsc.li/rsc-advances

Co doping is an effective means to improve the performance of Ni–Mn–Sn alloy bulks and thin films. However, the Co doping effect on the crystallization process of the Ni–Mn–Sn alloy thin films is important but not clear. Therefore, we investigate the influence of Co doping on the crystallization kinetics for $Ni_{50}Mn_{37-x}Sn_{13}Co_x$ (x = 0, 0.5, 1.5, 4) magnetic shape memory alloy thin films by DSC analysis. For the non-isothermal process, each DSC curve has a single exothermic peak, which is asymmetrical. The crystallization peak temperatures and the activation energy of thin films both rise gradually with increasing Co content. Then, the activation energy of $Ni_{50}Mn_{37-x}Sn_{13}Co_x$ (x = 0, 0.5, 1.5, 4) thin films obtained by the Kissinger equation method is determined as 157.9 kJ mol^{-1}, 198.8 kJ mol^{-1}, 213 kJ mol^{-1} and 253.6 kJ mol^{-1}, respectively. The local activation energy of thin films with different Co content show the different variation tendency. In the isothermal crystallization, the average of the Avrami exponent n for thin films of each Co content is approximately 1.5, suggesting that the mechanism of crystallization is two-dimensional diffusion-controlled growth for $Ni_{50}Mn_{37-x}Sn_{13}Co_x$ (x = 0, 0.5, 1.5, 4) thin films.

1. Introduction

The Ni–Mn–Sn magnetic shape memory alloys (MSMAs) have recently attracted considerable attention due to their unique properties and potential applications.[1–5] Researchers seek to add a fourth element to enhance the properties of Ni–Mn–Sn MSMAs, and it is found that Co addition has been shown to have an outstanding effect on the performance of Ni–Mn–Sn MSMAs, such as the magnetocaloric effect, magnetoresistance effect and elastocaloric effect.[6–9] Previously, Kainuma *et al.* obtained a huge magnetic-field-induced shape recovery strain of about 1.0% in the Ni–Co–Mn–Sn polycrystalline alloy, and it accompanied reverse martensitic transformation.[10] Some researchers also reported that the Co-doped in Ni–Mn–Sn alloys are an effective way to enhance the difference in magnetization between the martensite phase and austenite phase.[11–13] Recently, Cong *et al.* established the complete phase diagram of $Ni_{50-x}Co_xMn_{39}Sn_{11}$ alloys.[14]

Different from the bulk materials, the applications of Ni–Mn–Sn based alloys in micro-devices such as actuators, sensors, magnetic cooling, hybrid systems and magnetic driven micro-electromechanical systems (MEMS) need high quality thin films and even free-standing thin films.[15–17] Modak *et al.* have reported that refrigeration capacity (RC) and magnetic entropy change (ΔS_m) increased by Co addition in Ni–Mn–Sn thin films.[18] Ramudu *et al.* found a relatively large exchange bias effect (EBE) in Ni–Mn–Sn–Co thin films.[19] So far, Ni–Mn–Sn–Co alloy thin films are well studied and they can be properly used in the above-mentioned applications.

As we know, Ni–Mn–Sn based alloy thin films that prepared by magnetic sputtering at room temperature are usually amorphous alloys, which are at as-deposited state.[20–22] The shape memory effect, magnetocaloric effect and other significant properties cannot exhibit in the amorphous Ni–Mn–Sn based thin films. Therefore, it is a precondition that crystalline state of alloy thin films for investigating their properties and considering their practical application. Furthermore, the crystallization behavior exhibits the compositional sensitivity.[21] However, the influence of Co content on the crystallization behavior of Ni–Mn–Sn thin films is still unknown. Therefore, it is essential to investigate the effect of Co doping on the crystallization kinetics of Ni–Mn–Sn free-standing magnetic shape memory alloy thin films, which can be the foundation of following research.

In this study, for the first time, we focus on the influence of Co doping on the crystallization kinetics of $Ni_{50}Mn_{37-x}Sn_{13}Co_x$ (x = 0, 0.5, 1.5, 4) free-standing magnetic shape memory alloy thin films. Non-isothermal crystallization and isothermal crystallization of alloy thin films have been researched by Perkin-Elmer differential scanning calorimetric (DSC). In non-isothermal process, every DSC curve has one exothermic peak.

[a]School of Science, Harbin University of Science and Technology, Harbin 150080, China. E-mail: changlongtan@hrbust.edu.cn
[b]School of Materials Science and Engineering, Harbin Institute of Technology, Harbin 150001, China

The crystallization peak temperatures and activation energy of the Ni–Mn–Sn–Co thin films both rise gradually with increasing Co content. The local activation energy of thin films with different Co content show the different variation tendency. In the isothermal crystallization, the average of Avrami exponent n for thin films of each Co content are approximate 1.5, suggesting that the mechanism of crystallization is two-dimensional diffusion-controlled growth for $Ni_{50}Mn_{37-x}Sn_{13}Co_x$ ($x = 0$, 0.5, 1.5, 4) thin films. This study can elucidate the influence of Co content on the crystallization kinetics of Ni–Mn–Sn magnetic shape memory alloy thin films and provide guidance for designing and annealing process of thin films.

2. Experimental

The photoresist was deposited on silicon (100) substrate by spinning, and Ni–Mn–Sn–Co alloy thin films is deposited on photoresist and silicon substrate by dc magnetron sputtering from the $Ni_{50}Mn_{37}Sn_{13}$ sputtering target after setting working (Ar) gas pressure at 1.5×10^{-3} mbar and sputtering power at 100 W for 2 hours. Co is doped in the thin films by symmetrically placing Co wire on the Ni–Mn–Sn target. Later, the photoresist thin film is separated by acetone. The elemental composition of the Ni–Mn–Sn–Co free-standing thin films detected by energy dispersive X-ray analysis is found to be $Ni_{50}Mn_{37-x}Sn_{13}Co_x$ ($x = 0$, 0.5, 1.5, 4). The crystallization of thin films are determined by the Rigaku D/max-rb rotating anode X-ray diffraction meter (XRD) using Cu K radiation at room temperature. The microstructure of thin films is determined by atomic force microscope (AFM). Non-isothermal and isothermal crystallization of amorphous Ni–Mn–Sn–Co free-standing thin films samples are carried out on diamond differential scanning calorimetry (Diamond DSC, Perkin-Elmer). In the non-isothermal heating, a set of DSC plots is investigated at the heating rates of 10 K min^{-1}, 20 K min^{-1}, 30 K min^{-1}, 40 K min^{-1} and 60 K min^{-1}. In the isothermal analysis, the amorphous samples are firstly heated at a rate of 100 K min^{-1} to a fixed temperature (20 K below the crystallization temperature), then heated to the crystallization temperature at 20 K min^{-1}, finally held temperature for a few minutes, until completion of crystallization.

3. Results and discussion

Fig. 1 shows the room-temperature X-ray diffraction (XRD) patterns of $Ni_{50}Mn_{37-x}Sn_{13}Co_x$ ($x = 0$, 0.5, 1.5, 4) thin films after isothermal process. It is clear that all thin films show a typical diffraction cubic austenitic structure ($L2_1$), and the super lattice reflections such as the A(220) and A(422) peaks are observed.[23] It is also found that the super lattice reflections peaks of thin films has no significant difference with the increasing Co content, which is rather similar to the $Ni_{50}Mn_{37-x}Co_xSn_{13}$ reported by Yang.[24] The compositions of $Ni_{50}Mn_{37-x}Sn_{13}Co_x$ ($x = 0$, 0.5, 1.5, 4) thin films determined by EDX analysis were shown in Table 1.

Fig. 2 shows the microstructure of annealed $Ni_{50}Mn_{37-x}Sn_{13}Co_x$ ($x = 0$, 0.5, 1.5, 4) thin films determined by AFM. The size of selected area is 1 μm × 1 μm. The surface morphology of

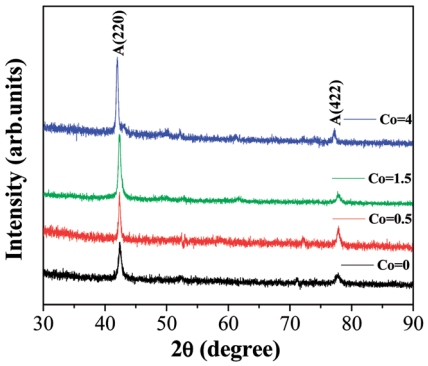

Fig. 1 XRD patterns of $Ni_{50}Mn_{37-x}Sn_{13}Co_x$ ($x = 0$, 0.5, 1.5, 4) thin films after isothermal process.

thin films is composed of defined grains, which demonstrate the thin films have fully crystallized. It can be clearly seen that the grain size decreases gradually with increasing Co content. In Fig. 2, it is found that the grains are unevenly distributed. This is because the motion of sputtering particles is uncontrollable, particles are randomly sputtered onto the substrate. The inset of Fig. 2 is the microstructure of as-deposited $Ni_{50}Mn_{37}Sn_{13}$ thin films shows disordered structure without any grains. It indicates that the as-deposited $Ni_{50}Mn_{37}Sn_{13}$ thin films are amorphous alloys.

Fig. 3 shows the DSC curves of $Ni_{50}Mn_{37-x}Sn_{13}Co_x$ ($x = 0$, 0.5, 1.5, 4) thin films obtained from the heating rates of 10 K min^{-1}, 20 K min^{-1}, 30 K min^{-1}, 40 K min^{-1} and 60 K min^{-1} in non-isothermal crystallization. Each DSC curve has a single exothermic peak, indicating that the occurrence of one-step crystallization. The exothermal peaks with different Co content are all moved to higher temperatures gradually with increasing heating rates. This manifests that the crystallization behavior is in a marked kinetic nature.[25–27] The values of the onset of crystallization temperature T_x and the crystallization peak temperature T_p for the different heating rates of samples are given in Table 2. It is found that the T_p are significantly shifted to higher temperatures with increasing Co content from Table 1. For example, the crystallization peak temperatures are determined at 542 K, 562.7 K, 568.7 K and 574.2 K at the heating rates of 40 K min^{-1}, respectively. This can be attributed to the grain refinement effect of Ni–Mn–Sn films.[28] From Fig. 2, the grain size of Ni–Mn–Sn–Co thin films decreases gradually with increasing Co content, which means the grain boundaries of thin films increase with increasing Co content. The plenty of grain boundaries can act as potential barriers. They separate the individual grains, and limit movement of atomics, thereby

Table 1 Compositions of $Ni_{50}Mn_{37-x}Sn_{13}Co_x$ ($x = 0$, 0.5, 1.5, 4) thin films determined by EDX analysis

Samples	Ni (at%)	Mn (at%)	Sn (at%)	Co (at%)
Co-0	50.05	36.93	13.02	0
Co-0.5	50.11	36.55	12.83	0.51
Co-1.5	49.96	35.41	13.11	1.52
Co-4	50.07	33.03	12.94	3.96

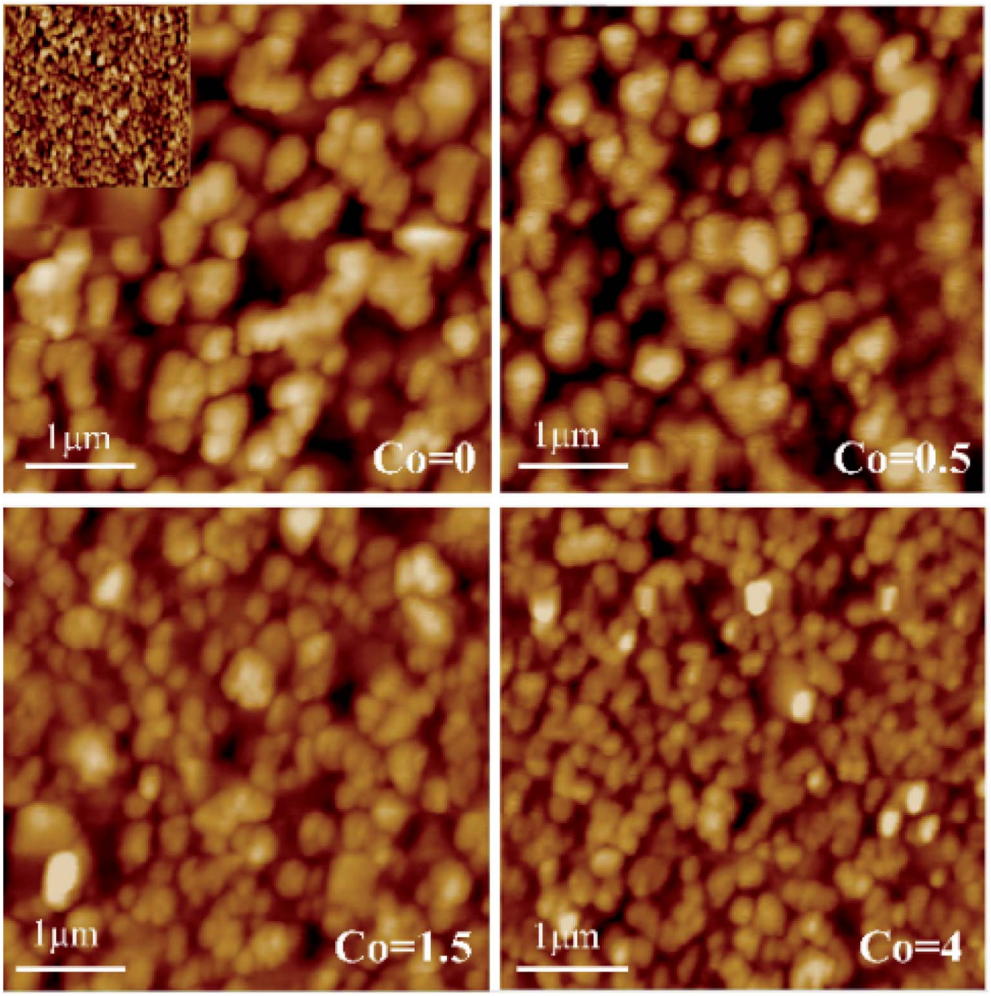

Fig. 2 AFM images of annealed $Ni_{50}Mn_{37-x}Sn_{13}Co_x$ (x = 0, 0.5, 1.5, 4) thin films, the inset is AFM image of as-deposited $Ni_{50}Mn_{37}Sn_{13}$ thin films.

imposing constraints on the nucleation and growth of crystallization process, such as crystallographic symmetry.[29] Thus, the crystallization peak temperatures T_p rise gradually with increasing Co content.

In the cause of further confirming the effects of Co addition on the crystallization kinetics of thin films, the activation energy of crystallization E_c is calculated. The E_c can be determined by the Kissinger equation:[30]

$$\ln(\beta/T_p^2) = -E_c/RT_p + \text{constants} \quad (1)$$

where T_p is the crystallization peak temperature, R is the gas constant, β is the heating rate. Therefore, the activation energy E_c of crystallization for $Ni_{50}Mn_{37-x}Sn_{13}Co_x$ (x = 0, 0.5, 1.5, 4) magnetic shape memory alloy thin films can be calculated from the slope of $\ln(\beta/T_p^2)$ *vs.* $1/T_p$. Fig. 4 shows the dashed lines obtained by plotting $\ln(\beta/T_p^2)$ *vs.* $1/T_p$ with each Co content. The activation energy E_c can be derived from the slope of these dashed lines.[31,32] With the Co content increases from 0 at%, 0.5 at%, 1.5 at% to 4 at%, the activation energy E_c is 157.9 kJ mol^{-1}, 198.8 kJ mol^{-1}, 213 kJ mol^{-1} and 253.6 kJ mol^{-1}, respectively. It is evident that the activation energy E_c increase with increasing Co content. This can be attributed to the microstructure of ternary Ni–Mn–Sn alloy thin films markedly changes. When the Mn atomic is substituted by Co atomic, the addition of Co changes the number of grain boundaries of Ni–Mn–Sn alloy thin films, the grain refinement effect of the thin films is obvious, and the activation energy E_c of thin films rise with increasing Co content. Moreover, there is few theoretical basis for the change of activation energy. Some researchers tried to explain this by e/a before. Here, we consider that the change of activation energy is related to the phase stability. We consider to calculate the bind energy by first principles calculation to determine the phase stability. Thus, the relation between the phase stability and activation energy will be established. This work has a great research value and will be carried out in our further study.

Fig. 5 shows the plots of the relation between temperature and crystallized volume fraction of $Ni_{50}Mn_{37-x}Sn_{13}Co_x$ (x = 0, 0.5, 1.5, 4) magnetic shape memory alloy thin films at different heating rates severally. It is found that temperature-crystallized volume fraction curves are mainly sigmoid curves in each Co content. It indicates that crystallization process of $Ni_{50}Mn_{37-x}Sn_{13}Co_x$ (x = 0, 0.5, 1.5, 4) thin films are not surface

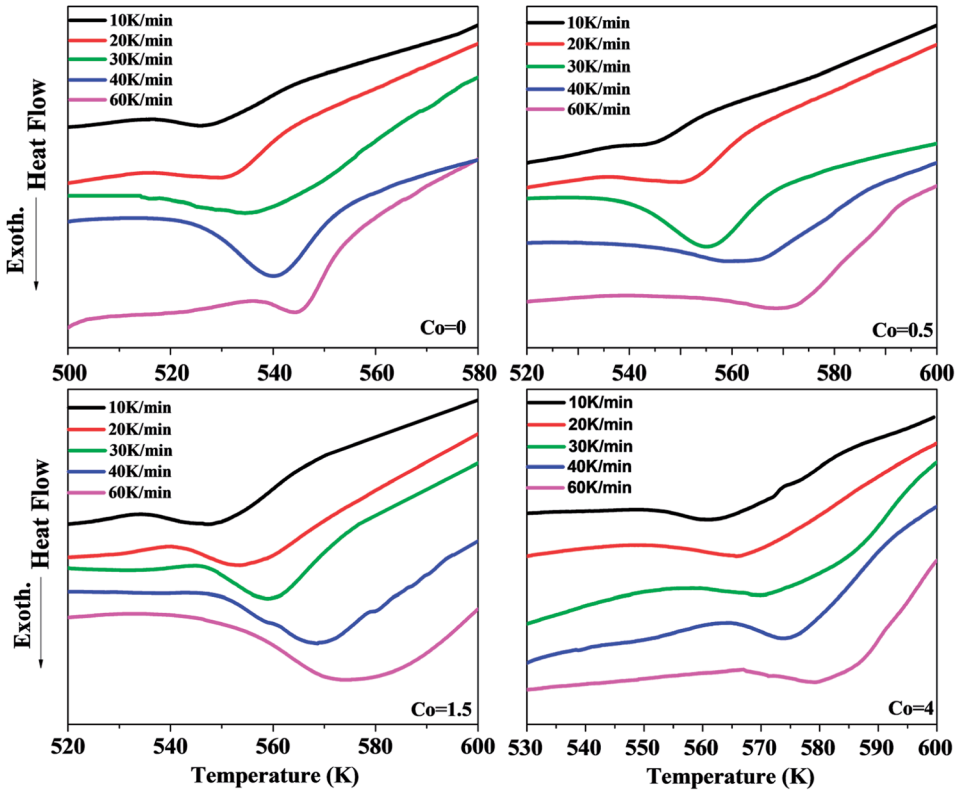

Fig. 3 DSC curves of $Ni_{50}Mn_{37-x}Sn_{13}Co_x$ (x = 0, 0.5, 1.5, 4) thin films obtained from different heating rates, respectively.

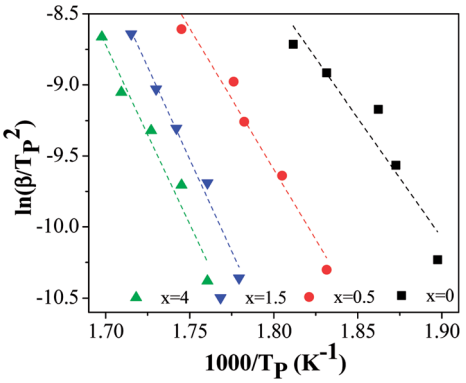

Fig. 4 Plot of $\ln(\beta/T_p^2)$ *vs.* $1000/T_p$ for the $Ni_{50}Mn_{37-x}Sn_{13}Co_x$ (x = 0, 0.5, 1.5, 4) thin films.

crystallization but bulk crystallization.[33] As shown in Fig. 5, the curves shift to the higher temperature gradually with the increase of Co content.

The activation energy obtained from Kissinger equation is apparent activation energy. The apparent activation energy represent the average of activation energy in the whole crystallization process. The activation energy is diverse because the different stages of crystallization have the different mechanism of nucleation and growth. Thus, for purpose of reflecting the change of activation energy, it is essential to investigate the local activation energy. Therefore, the local activation energy of $Ni_{50}Mn_{37-x}Sn_{13}Co_x$ (x = 0, 0.5, 1.5, 4) free-standing thin films are calculated by Doyle method. Its relation is[34]

$$\lg B = \lg\frac{AE}{RF(x)} - 2.315 - 0.4567\frac{E}{RT} \quad (2)$$

where A is the frequency factor, B is the heating rate, T is the temperature, x is the crystallized volume fraction, R is the gas constant, and $F(x)$ is a crystallization function that relate to x.

Fig. 6 shows the local activation energy $E_c(\alpha)$ *versus* the crystallized volume fraction α of the $Ni_{50}Mn_{37-x}Sn_{13}Co_x$ (x = 0, 0.5, 1.5, 4) free-standing thin films. From Fig. 5, we can found that the $E_c(\alpha)$ of thin films with different Co content show the different variation tendency. As Co = 0, $E_c(\alpha)$ increase with increasing crystallized volume fraction. As Co = 0.5 and 1.5, $E_c(\alpha)$ decrease with increasing crystallized volume fraction. As Co = 4, $E_c(\alpha)$ basically remains at 250 kJ mol^{-1}. It indicates that the α has obvious influence on the variation of $E_c(\alpha)$, and the crystallization mechanism of $Ni_{50}Mn_{37-x}Sn_{13}Co_x$ (x = 0, 0.5, 1.5, 4) thin films changed constantly. The average of local activation energy with each Co content calculated by Doyle method is close to the apparent activation energy obtained from Kissinger's equation, indicating that the activation energy calculated by two methods have little error.

In order to investigate the effect of Co content on the nucleation and growth of crystallization process, the isothermal crystallization process of $Ni_{50}Mn_{37-x}Sn_{13}Co_x$ (x = 0, 0.5, 1.5, 4) magnetic shape memory alloy thin films were also observed. Fig. 7 shows a set of the isothermal DSC curves of $Ni_{50}Mn_{37-x}Sn_{13}Co_x$ (x = 0, 0.5, 1.5, 4) thin films at each corresponding temperatures, respectively. The isothermal crystallization temperature of thin films with each Co content

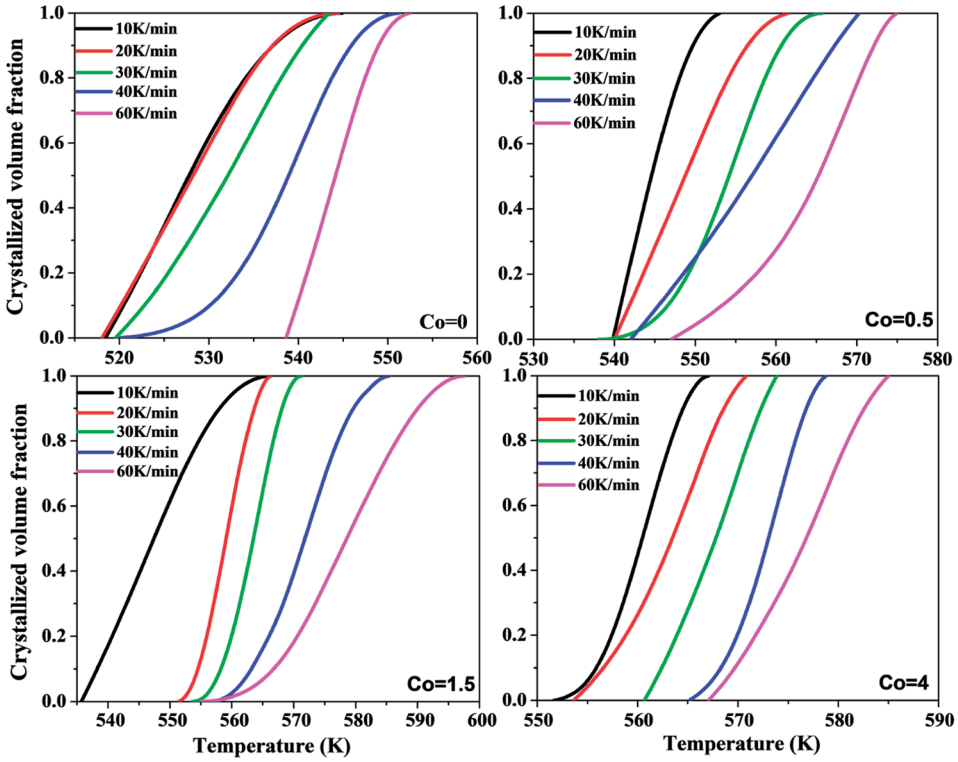

Fig. 5 Plots of the relation between crystallized volume fraction and temperature of $Ni_{50}Mn_{37-x}Sn_{13}Co_x$ (x = 0, 0.5, 1.5, 4) thin films.

are selected below the non-isothermal crystallization temperature at 10 K min^{-1} with each corresponding Co content, in order to ensure the completion of full crystallization. The single exothermic peaks of all DSC curves appeared after passing a certain incubation time. The incubation time decreases with increasing isothermal temperature. It implies that the crystallization process is influenced by the isothermal temperatures.[21]

In order to reveal the crystallization mechanism of $Ni_{50}Mn_{37-x}Sn_{13}Co_x$ (x = 0, 0.5, 1.5, 4) free-standing thin films, the plots of crystallized volume fraction-isothermal time for

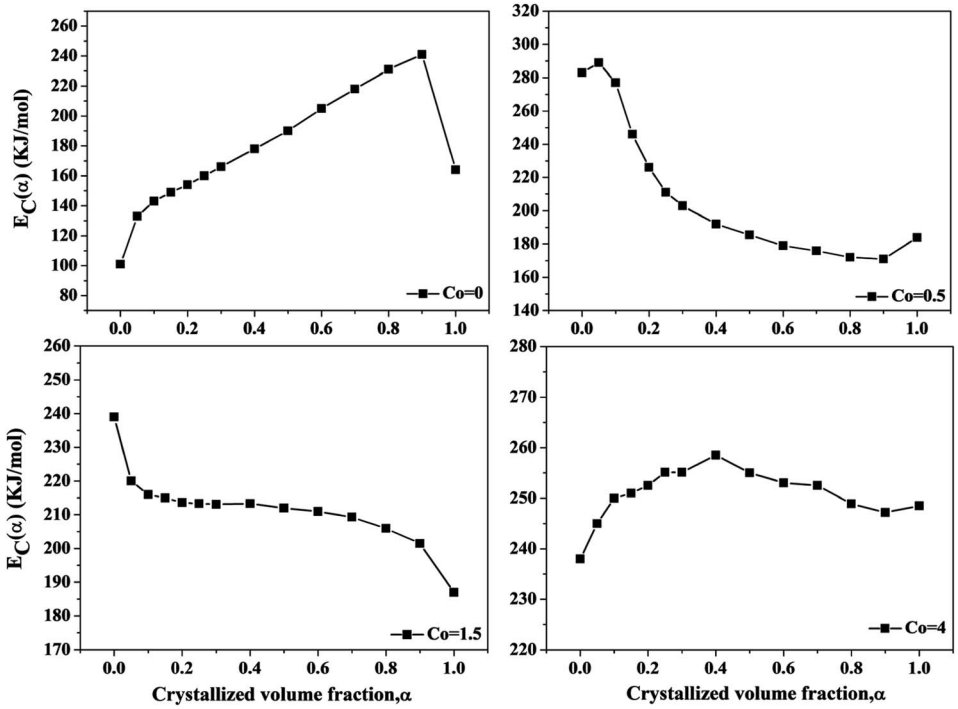

Fig. 6 The local activation energy *versus* the crystallized volume fraction α of $Ni_{50}Mn_{37-x}Sn_{13}Co_x$ (x = 0, 0.5, 1.5, 4) thin films.

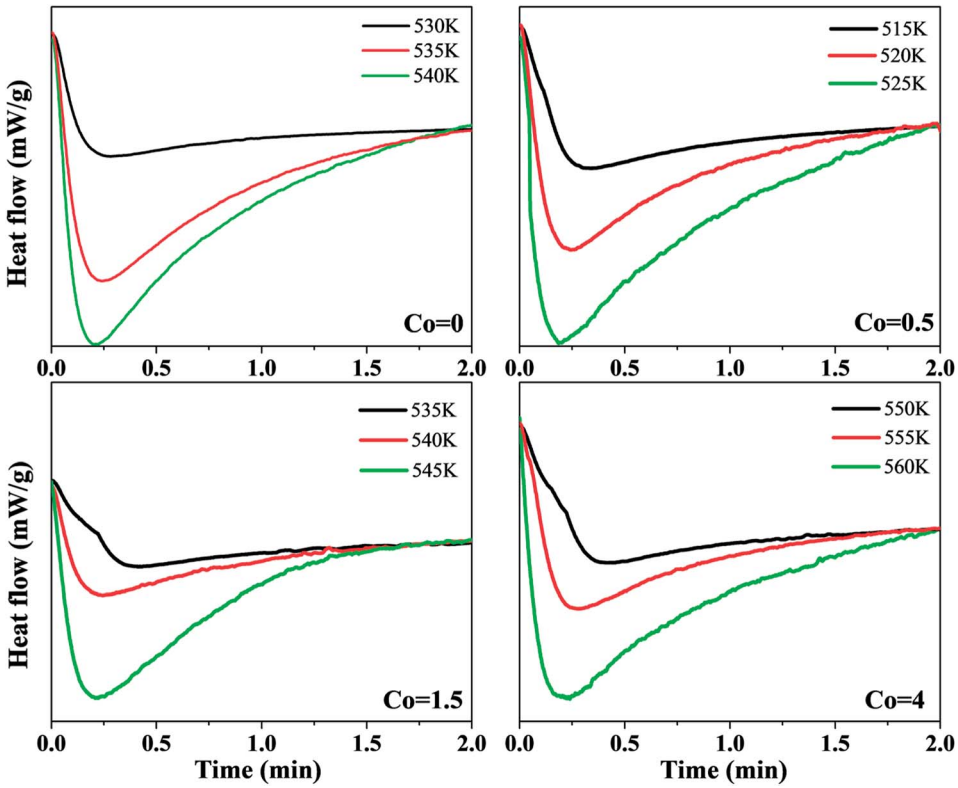

Fig. 7 Isothermal DSC curves of $Ni_{50}Mn_{37-x}Sn_{13}Co_x$ (x = 0, 0.5, 1.5, 4) thin films at different temperatures.

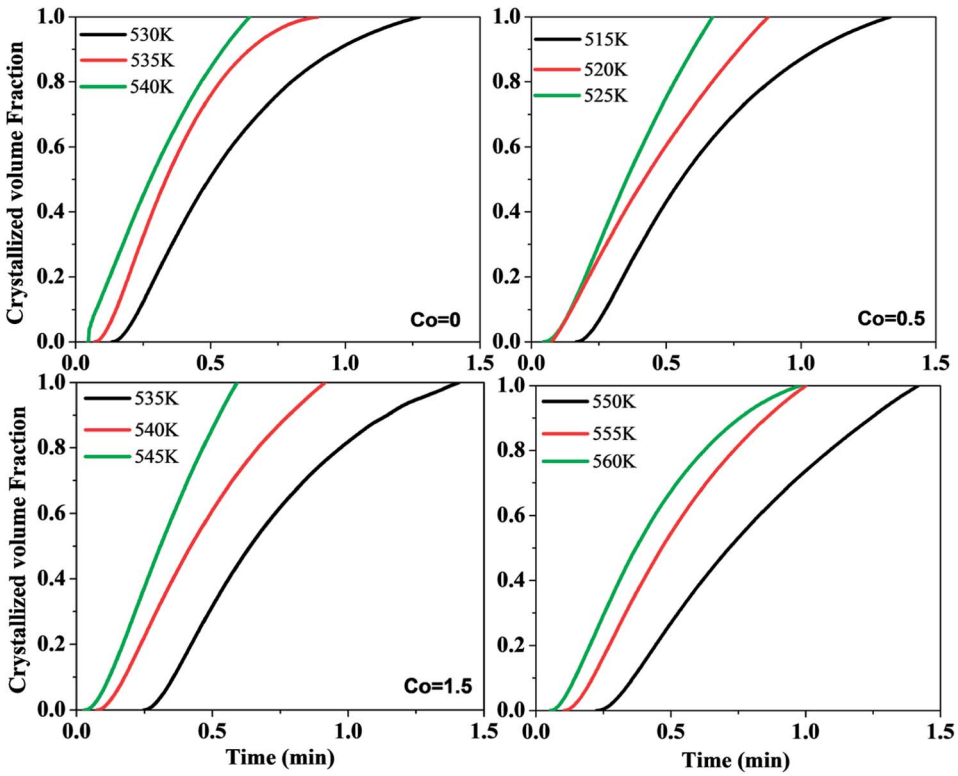

Fig. 8 Plots of crystallized volume fraction–time curves for $Ni_{50}Mn_{37-x}Sn_{13}Co_x$ (x = 0, 0.5, 1.5, 4) thin films in isothermal crystallization.

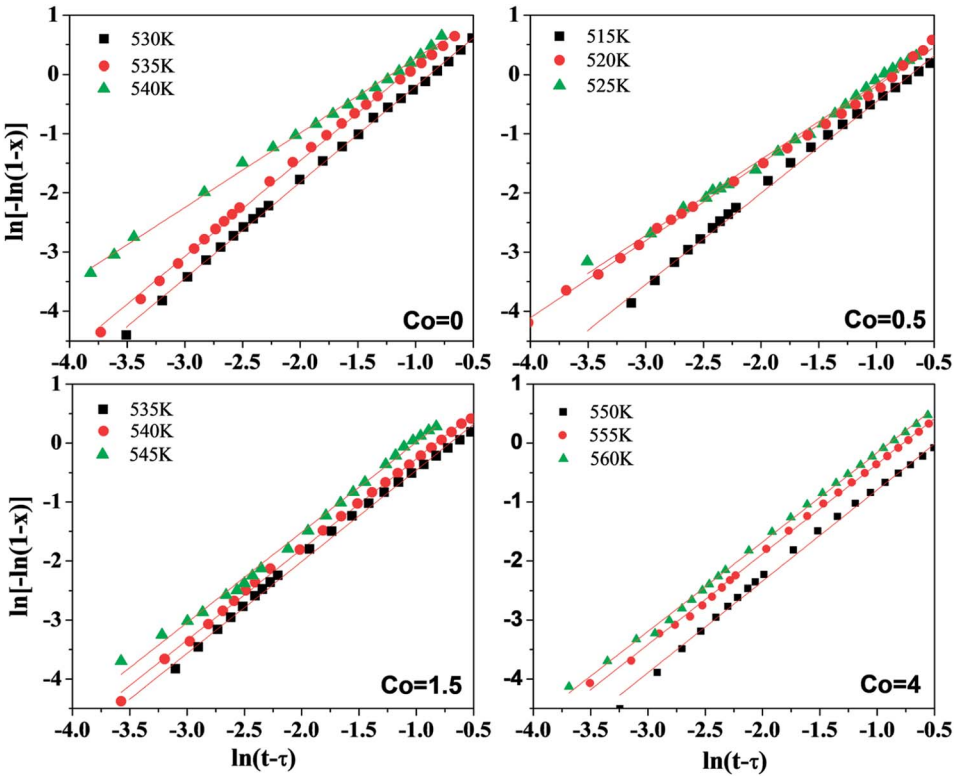

Fig. 9 The JMA plots for the isothermal crystallization of the $Ni_{50}Mn_{37-x}Sn_{13}Co_x$ (x = 0, 0.5, 1.5, 4) thin films at different crystallization temperatures.

Table 2 Values of T_x and T_p determined at different heating rates for the $Ni_{50}Mn_{37-x}Sn_{13}Co_x$ (x = 0, 0.5, 1.5, 4) thin films

	Co_0		$Co_{0.5}$		$Co_{1.5}$		Co_4	
Heating rates (K min^{-1})	T_x (K)	T_p (K)	T_x (K)	T_p (K)	T_x (K)	T_p (K)	T_x (K)	T_p (K)
10	519	525.8	539	545.8	535	547	551	561
20	517	531.1	537	551.7	541	553.7	553	566.4
30	514	535.1	538	555.3	545	559	554	570
40	518	540	539	562.7	548	568.7	565	574.2
60	535	544.8	539	569.2	543	575.7	566	579.1

$Ni_{50}Mn_{37-x}Sn_{13}Co_x$ (x = 0, 0.5, 1.5, 4) thin films in isothermal crystallization are shown in Fig. 8. From Fig. 8, almost all curves are sigmoidal. Then, crystallization kinetics can be analyzed by the theoretical Johnson–Mehl–Avrami (JMA) equations:[35]

$$\ln[-\ln(1-x)] = n\ln k + n\ln(t-\tau) \quad (3)$$

where x is crystallized volume fraction, n is the Avrami exponent which reflects the mechanism of nucleation and growth, τ is the incubation time, k is the reaction rate and k follows the Arrhenius relation:

$$k = A\exp\left(-\frac{E_A}{RT}\right) \quad (4)$$

here A is a constant. E_A is the activation energy of isothermal crystallization.

Fig. 9 shows the plots of $\ln[\ln(1/1-x)]$ *versus* $\ln(t-\tau)$ at corresponding temperature of $Ni_{50}Mn_{37-x}Sn_{13}Co_x$ (x = 0, 0.5, 1.5, 4) free-standing thin films. Evidently, the data of $\ln[\ln(1/1-x)]$ *versus* $\ln(t-\tau)$ are approximate to straight lines, and the value of Avrami exponent n could be obtained from the slope in Fig. 9. The data of 5% < x < 90% are almost on a straight line, a slight deviation in linearity can be put down to the non-steady nucleation in the final stage of crystallization.[26] The Avrami exponents at different temperatures are shown in Table 3. The

Table 3 Avrami exponent n of the $Ni_{50}Mn_{37-x}Sn_{13}Co_x$ (x = 0, 0.5, 1.5, 4) thin films during isothermal crystallization

Avrami exponent n			
Co_0	$Co_{0.5}$	$Co_{1.5}$	Co_4
1.62	1.59	1.56	1.55
1.42	1.39	1.53	1.52
1.26	1.28	1.50	1.51

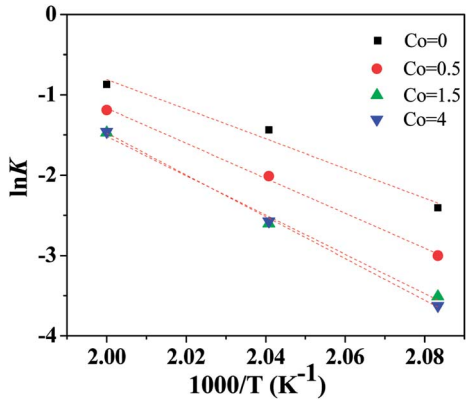

Fig. 10 Plot of ln$k$ *vs.* 1000/T of $Ni_{50}Mn_{37-x}Sn_{13}Co_x$ (x = 0, 0.5, 1.5, 4) thin films for isothermal crystallization process.

Avrami exponents n for all $Ni_{50}Mn_{37-x}Sn_{13}Co_x$ (x = 0, 0.5, 1.5, 4) thin films are mainly in the range of 1.3 to 1.6. Averaging the n of each Co content respectively, the average of Avrami exponent for each Co content are all nearly 1.5. On the basis of the relation between the crystallization mechanism of nucleation and growth and Avrami exponent n in isothermal conditions,[35–38] it can be found that the main mechanism of nucleation and growth for $Ni_{50}Mn_{37-x}Sn_{13}Co_x$ (x = 0, 0.5, 1.5, 4) thin films are all diffusion-controlled two-dimensional growth. Co content has a small influence on the crystallization mechanism of $Ni_{50}Mn_{37-x}Sn_{13}Co_x$ (x = 0, 0.5, 1.5, 4) free-standing thin films.

Moreover, we have a discussion about the process of nucleation. Firstly, the alloy nucleates by diffusion-control near the small number of clusters that formed during the formation of amorphous structures preferentially at a certain temperature. With the increase of temperature or the extension of time, the small clusters formed by a large number of atoms nucleates by diffusion-control successively. The small clusters that near the preferential-formed nucleus grow up gradually, until all grains form and end up with colliding with each other.

Fig. 10 shows the plot of ln$k$ *vs.* 1000/T of $Ni_{50}Mn_{37-x}Sn_{13}Co_x$ thin films for isothermal crystallization process. According to eqn (4), the activation energy E_A can be calculated by the slope of ln$k$ *vs.* 1000/T. With increase of Co content, the E_A is 152.3 kJ mol^{-1}, 171.3 kJ mol^{-1}, 220.2 kJ mol^{-1} and 229.8 kJ mol^{-1}, respectively. These values of E_A obtained by JMA equation are close to the E_c calculated from Kissinger equations, implying that the mechanism of two crystallization methods are similar for $Ni_{50}Mn_{37-x}Sn_{13}Co_x$ (x = 0, 0.5, 1.5, 4) thin films.

The crystallization process can exhibit different nucleation and growth behavior at different stages. Thus, in order to study the details of crystallization mechanism, it is essential to investigate the local Avrami exponent of crystallization process. Radlinski and Calka have suggested an analysis method for isothermal DSC, which can obtain the local Avrami exponent $n(x)$ with crystallized volume fraction x efficiently.[39] The local Avrami exponent $n(x)$ can be calculated by the following equation:

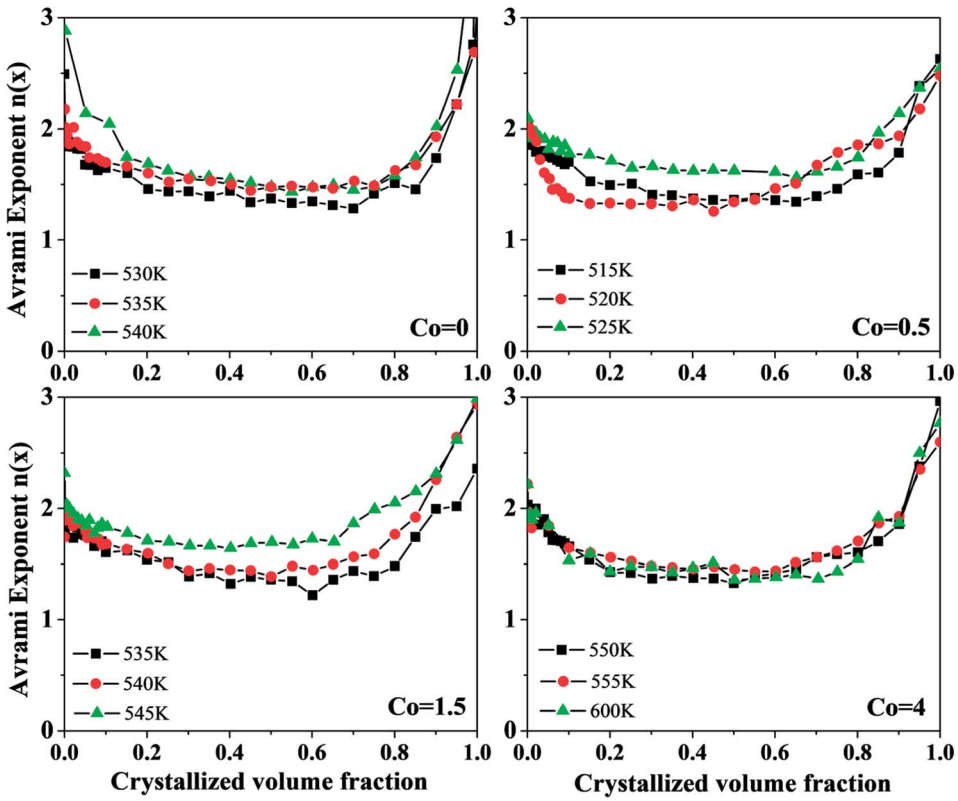

Fig. 11 The local Avrami exponents $n(x)$ *versus* crystallized volume fraction of $Ni_{50}Mn_{37-x}Sn_{13}Co_x$ (x = 0, 0.5, 1.5, 4) thin films.

$$n(x) = \frac{d\ln[-\ln(1-x)]}{d\ln(t-\tau)} \quad (5)$$

Fig. 11 shows the local Avrami exponents $n(x)$ *versus* crystallized volume fraction x at different temperatures of $Ni_{50}Mn_{37-x}Sn_{13}Co_x$ ($x = 0$, 0.5, 1.5, 4) thin films. It can be seen that the change of local Avrami exponents $n(x)$ with different Co content is roughly similar. They all first decrease, then tend to be flat, and rise rapidly in the end. It implies that the change in Co content has a small influence on the crystallization mechanism of $Ni_{50}Mn_{37-x}Sn_{13}Co_x$ ($x = 0$, 0.5, 1.5, 4) thin films. The local Avrami exponent $n \approx 2$ in the beginning, and decreased from 2 to 1.5 in the range of $0 < x < 0.2$. Then, the local Avrami exponent stays around 1.5 in the range of $0.2 < x < 0.8$. Finally, the local Avrami exponent quick rises to 3 in the range of $0.8 < x < 1$. Therefore, the crystallization process is divided into three stages approximately: in the first stage that x ranges from 0 to 0.2, implying the mechanism of nucleation and growth is diffusion-controlled two-dimensional growth, and the nucleation rate decreased in this stage. x ranges from 0.2 to 0.8 in the second stage, implying that the crystallization mechanism is diffusion-controlled two-dimensional growth, and the nucleation rate is zero. x ranges from 0.8 to 1 in the third stage, implying that the crystallization mechanism is diffusion-controlled three-dimensional growth, and the nucleation rate increases. The variation of local Avrami exponents $n(x)$ demonstrates that the mechanism of nucleation and growth for $Ni_{50}Mn_{37-x}Sn_{13}Co_x$ ($x = 0$, 0.5, 1.5, 4) free-standing thin films changes constantly.

4. Conclusions

In conclusion, the effects of Co doping on the crystallization kinetics of $Ni_{50}Mn_{37-x}Sn_{13}Co_x$ ($x = 0$, 0.5, 1.5, 4) free-standing magnetic shape memory alloy thin films have been investigated by using XRD analysis, AFM analysis, non-isothermal and isothermal DSC analysis. $Ni_{50}Mn_{37-x}Sn_{13}Co_x$ ($x = 0$, 0.5, 1.5, 4) thin films are typical cubic austenitic structure ($L2_1$). The grain size of thin films decreases gradually with increasing Co content. In non-isothermal crystallization, the activation energy calculated by Kissing's method is 157.9 kJ mol^{-1}, 198.8 kJ mol^{-1}, 213 kJ mol^{-1} and 253.6 kJ mol^{-1}, respectively. The crystallization peak temperatures and apparent activation energy both rise gradually with increasing Co content, which could be due to the fact that Co doping changes the number of grain boundaries of Ni–Mn–Sn alloy thin films. The local activation energy of thin films with different Co content show the different variation tendency. In isothermal crystallization, the isothermal temperatures influence the crystallization process of $Ni_{50}Mn_{37-x}Sn_{13}Co_x$ ($x = 0$, 0.5, 1.5, 4) thin films. The average of Avrami exponent n for thin films of each Co content is approximately 1.5. The activation energies obtained in non-isothermal crystallization and isothermal crystallization are close, implying that the mechanisms of the two crystallization methods are similar. The variation of local Avrami exponents $n(x)$ demonstrates that the crystallization mechanism of $Ni_{50}Mn_{37-x}Sn_{13}Co_x$ ($x = 0$, 0.5, 1.5, 4) thin films changes constantly, from diffusion-controlled two-dimensional growth to diffusion-controlled three-dimensional growth. The nucleation rate decreases firstly, then remains zero for some time, and finally increases.

Conflicts of interest

There are no conflicts to declare.

Acknowledgements

The authors acknowledge the supports of National Natural Science Foundation of China (Grant No. 51471064 and 51301054); and Program for Youth Academic Backbone in Heilongjiang Provincial University (Grant No. 1251G022).

References

1 Y. Sutou, Y. Imano, N. Koeda, T. Omori, R. Kainuma, K. Ishida and K. Oikawa, *Appl. Phys. Lett.*, 2004, **85**, 4358–4360.
2 K. Ullakko, J. K. Huang, C. Kantner, R. C. O'Handley and V. V. Kokorin, *Appl. Phys. Lett.*, 1996, **69**, 1966–1968.
3 N. Teichert, A. Auge, E. Yüzüak, I. Dincer, Y. Elerman, B. Krumme, H. Wende, O. Yildirim, K. Potzger and A. Hüzütten, *Acta Mater.*, 2015, **86**, 279–285.
4 R. Modak, B. Samantaray, P. Mandal and A. Srinivasan, *Appl. Phys. A*, 2016, **122**, 1–7.
5 T. Krenke, M. Acet, E. F. Wassermann, X. Moya, L. Manosa and A. Planes, *Phys. Rev. B: Condens. Matter Mater. Phys.*, 2005, **72**, 014412.
6 C. Jing, Z. Li, H. L. Zhang, J. P. Chen and Y. F. Qiao, *Eur. Phys. J. B*, 2009, **67**, 193–196.
7 H. S. Liu, C. L. Zhang, Z. D. Han, H. C. Xuan and D. H. Wang, *J. Alloys Compd.*, 2009, **467**, 27–30.
8 Z. Han, D. Wang, B. Qian, J. Feng and X. Jiang, *Jpn. J. Appl. Phys.*, 2010, **49**, 0211.
9 Z. Yang, D. Y. Cong, L. Huang, Z. H. Nie and X. M. Sun, *Mater. Des.*, 2015, **92**, 932–936.
10 R. Kainuma, Y. Imano, W. Ito, H. Morito, Y. Sutou, K. Oikawa, A. Fujita and K. Ishida, *Appl. Phys. Lett.*, 2006, **88**, 192513.
11 W. Ito, X. Xu, R. Y. Umetsu, T. Kanomata, K. Ishida and R. Kainuma, *Appl. Phys. Lett.*, 2010, **97**, 242512.
12 R. Y. Umetsu, A. Sheikh, W. Ito, B. Ouladdiaf, K. R. A. Ziebeck, T. Kanomata and R. Kainuma, *Appl. Phys. Lett.*, 2011, **98**, 042507.
13 D. Y. Cong, S. Roth, M. Potschke, C. Hurrich and L. Schultz, *Appl. Phys. Lett.*, 2010, **97**, 1966.
14 D. Y. Cong, S. Roth and L. Schultz, *Acta Mater.*, 2012, **60**, 5335–5351.
15 K. Bhattacharya and R. D. James, *J. Mech. Phys. Solids*, 1999, **47**, 531–576.
16 J. W. Dong, J. Q. Xie, J. Lu, C. Adelmann, C. J. Palmstrøm, J. Cui, Q. Pan, T. W. Shield, R. D. James and S. McKernan, *J. Appl. Phys.*, 2004, **95**, 2593–2600.

17 B. Winzek, S. Schmitz, H. Rumpf, T. Sterzl, R. Hassdorf, S. Thienhaus, J. Feydt, M. Moske and E. Quandt, *Mater. Sci. Eng., A*, 2004, **378**, 40–46.
18 R. Modak, M. M. Raja and A. Srinivasan, *J. Magn. Magn. Mater.*, 2017, **448**, 146–152.
19 R. Machavarapu and G. Jakob, *Appl. Phys. Lett.*, 2013, **102**, 232406.
20 Z. Wang, E. Guo, C. Tan, X. Tian, W. Cai and J. Zhu, *RSC Adv.*, 2017, **7**, 42866–42874.
21 X. H. Tian, Z. H. Wang, J. C. Zhu, C. L. Tan, K. Zhang, Z. Yu and W. Cai, *J. Non-Cryst. Solids*, 2018, **495**, 19–26.
22 R. Vishnoi and D. Kaur, *Surf. Coat. Technol.*, 2010, **204**, 3773–3782.
23 S. E. Muthu, N. V. R. Rao, M. M. Raja, D. M. R. Kumar, D. M. Radheep and S. Arumugam, *J. Phys. D: Appl. Phys.*, 2010, **43**, 425002.
24 L. H. Yang, H. Zhang, F. X. Hu, J. R. Sun, L. Q. Pan and B. G. Shen, *J. Alloys Compd.*, 2014, **588**, 46–48.
25 J. Z. Chen and S. K. Wu, *Thin Solid Films*, 1999, **339**, 194–199.
26 Z. Z. Yuan, X. D. Chen, B. X. Wang and Z. J. Chen, *J. Alloys Compd.*, 2005, **399**, 166–172.
27 S. Venkataraman, J. Eckert, L. Schultz and D. J. Sordelet, *Intermetallics*, 2016, **14**, 1085–1090.
28 A. L. Alves, E. C. Passamani, V. P. Nascimento and A. Y. Takeuchi, *J. Phys. D: Appl. Phys.*, 2010, **43**, 227–238.
29 R. Vishnoi and D. Kaur, *Surf. Coat. Technol.*, 2010, **204**, 3773–3782.
30 H. E. Kissinger, *Anal. Chem.*, 1957, **29**, 1702–1706.
31 S. K. Wu, K. H. Tseng and J. Y. Wang, *Thin Solid Films*, 2002, **408**, 316–320.
32 T. Hysen, T. Senoy, R. V. Ramanujan and M. R. Anantharaman, *J. Mater. Sci.*, 2008, **43**, 635–640.
33 A. A. Pratap, K. N. Lad, T. L. S. Rao, P. Majmudar and N. S. Saxena, *J. Non-Cryst. Solids*, 2004, **345**, 178–181.
34 C. D. Doyle, *J. Appl. Polym. Sci.*, 1961, **5**, 1845–1864.
35 M. Avrami, *J. Chem. Phys.*, 1939, **7**, 1103–1112.
36 M. Avrami, *J. Chem. Phys.*, 1940, **8**, 212–224.
37 M. Avrami, *J. Chem. Phys.*, 1941, **9**, 177–184.
38 J. Málek, *Thermochim. Acta*, 1995, **267**, 61–73.
39 A. Calka and A. P. Radlinski, *J. Mater. Res.*, 1985, **3**, 59.